Systematic Design and Parametric Analysis of GaN Vertical Trench MOS Barrier Schottky Diode With p-GaN Shielding Rings

Sihao Chen, Hang Chen, Yingbin Qiu, and Chao Liu

***Abstract*— We report GaN vertical trench MOS barrier Schottky (TMBS) diodes with embedded p-GaN shielding rings (SRs) and systematically investigate the impact of different structural parameters of the p-GaN SRs on the breakdown performance of the GaN-based vertical TMBS diodes by numerical simulation. The charge coupling effect by the embedded p-n junction at the bottom of the trench homogenize the electric field at the trench corner and alleviate the electric field crowding effect at the Schottky contact region, which can effectively avoid the premature breakdown and improve the reverse blocking capability of the TMBS diodes. The p-GaN SRs can also broaden the overlapped depletion region and shift the pinch-off point into the n^--GaN drift region, thus facilitating the 2-D depletion in the n^--GaN drift layer and boosting the breakdown performance of the conventional TMBS diodes. We found that the doping concentration, thickness, and the width of the p-GaN SRs are closely associated with the electric field distribution and the reverse breakdown characteristics of the GaN-based vertical TMBS diodes. The vertical TMBS diodes with optimal p-GaN SR parameters featured a dramatic improvement in the breakdown voltage from 907 to 1281 V, without an obvious degradation in the ON performance. The proposed TMBS diodes with a p-GaN SR structure can pave the way toward a high-performance GaN vertical power device for high-power and high-efficiency power switch applications.**

***Index Terms*— Breakdown voltage (BV), device design, gallium nitride, specific ON-resistance, vertical trench MOS barrier Schottky (TMBS) diode.**

I. Introduction

GaN-BASED power electronic devices have emerged as one of the most prominent candidates for high-power and high-voltage applications, for example, fast charging, mobile communication, data centers, and renewable energy. Recent studies demonstrated lateral GaN power devices with large breakdown voltage (BV) and low ON-resistance, thanks to the high-density 2-D electron gas (2DEG) formed at the AlGaN/GaN interface [1]–[5]. However, the footprint and parasitic components of the lateral devices scale proportionally with the BV, which can result in a limited switching frequency of the devices for high-voltage (>650 V) and high-current applications [6]–[8]. Moreover, the 2DEG channel of the lateral device locates in the vicinity of the device surface, making it extremely vulnerable to the surface states [9]. Fortunately, GaN vertical devices are not plagued by these issues. A high breakdown vertical device can be made possible by simply increasing the vertical thickness of the drift layer, without increasing the footprint of the devices. The ON-state current flows through the bulk material instead of the near-surface 2DEG channels and thus a more reliable dynamic performance can be achieved with a vertical device topology [10]–[15].

Schottky barrier diodes (SBDs) are one of the most important components of modern power systems due to its low voltage drop and fast switching capability [16]–[21]. Nevertheless, GaN-based diodes are not yet commercially available, probably due to the dynamic and reliability issues related to the lateral architectures. Given the unique advantages over their lateral counterparts, GaN vertical SBDs are recognized as promising alternatives for the next-generation power modules and systems. However, suffering from the energy barrier lowering effect induced by the image force, GaN vertical SBDs are bedeviled by severe reverse leakage current at reverse bias condition, which results in premature breakdown of the device and undesirable power consumption of the power systems in the OFF state [22].

Extensive research has been conducted to tackle the reverse leakage and premature breakdown issue. A vertical junction barrier Schottky (JBS) structure was proposed and proved to be effective [23]–[25]. Another way to improve the reverse characteristics is to employ a vertical trench MOS barrier Schottky (TMBS) structure. The TMBS diode design adopts a MOS structure to shield the electric field at the Schottky interface. As a result, the reverse leakage current caused by the image force can be alleviated [26]. However, a strong electric field crowding effect is commonly observed at the corner of the trench, which limits or even degrades the

Manuscript received July 14, 2021; revised August 24, 2021; accepted August 25, 2021. Date of publication September 14, 2021; date of current version October 22, 2021. This work was supported in part by the Guangdong Basic and Applied Basic Research Foundation under Grant 2020A1515111018, in part by the Shandong Provincial Natural Science Foundation under Grant ZR2020QF079, in part by the Qilu Young Scholar Program under Grant 11500089963075, and in part by the Center of Nanoelectronics, Shandong University, China. The review of this article was arranged by Editor P. J. Fay. *(Corresponding author: Chao Liu.)*

Sihao Chen, Hang Chen, and Chao Liu are with the School of Microelectronics, Institute of Novel Semiconductors, Shandong Technology Center of Nanodevices and Integration, State Key Laboratory of Crystal Materials, Shandong University, Jinan 250100, China, and also with the Shenzhen Research Institute, Shandong University, Shenzhen 518057, China (e-mail: chao.liu@sdu.edu.cn).

Yingbin Qiu is with Crosslight Software Inc., Shanghai 200063, China.

Color versions of one or more figures in this article are available at https://doi.org/10.1109/TED.2021.3109845.

Digital Object Identifier 10.1109/TED.2021.3109845

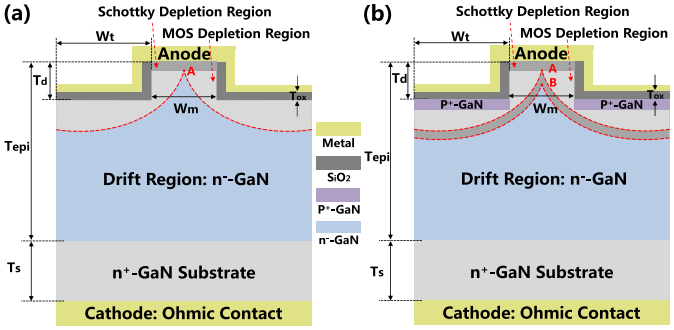

Fig. 1. Cross-sectional schematic of (a) conventional GaN-based TMBS diodes and (b) GaN-based TMBS with p-GaN SRs.

breakdown capability of the TMBS diodes [27]–[31]. Recently, Zhang *et al.* [31] demonstrated improved breakdown characteristics of GaN vertical TMBS diodes with argon (Ar) implanted shielding rings (SRs) at the bottom of the trench. The improved breakdown performance can be attributed to the redistribution of the electric field by incorporating the SRs, whereas the impact of the structural parameters of the SRs on the device performance and the theoretical limit of the SR-TMBS diodes remains to be explored. Moreover, an enhanced charge coupling effect from the SRs can be anticipated by replacing the Ar-doped GaN with Mg-doped p-type GaN, which can form an embedded p-n junction and promote the 2-D depletion toward the n^--GaN drift region. In this article, we report GaN-based TMBS diodes with p-GaN SRs and systematically investigated the impact of key structural parameters (e.g., the doping concentration, thickness, and width) of the p-GaN SRs on the forward and reverse characteristics of the GaN-based vertical TMBS diodes. With optimum p-GaN SRs, the BV of the TMBS diodes can be boosted from 907 to 1281 V, without degrading the ON performance of the devices. These results reveal great potential of GaN vertical SR-TMBS diodes for high-efficiency and high-frequency power switch applications.

II. Device Architectures and Parameters

Fig. 1(a) and (b) illustrate cross-sectional schematics for the conventional TMBS (C-TMBS) diodes and proposed TMBS diodes with p-GaN SRs (SR-TMBS), respectively. Both devices consist of trench MOS structures with a 9-μm-thick n^--GaN drift layer (Si $= 2 \times 10^{16}$ cm^{-3}) on an n^+-GaN substrate (Si $= 5 \times 10^{18}$ cm^{-3}), except that p-GaN SRs were incorporated beneath the trench of the SR-TMBS diodes. As shown in Fig. 1(a), depletion region occurs underneath the Schottky contact and along the vertical sidewall of the MOS structures under the reverse bias condition. As the reverse bias increases, an overlap of the depletion region by the two adjacent MOS structures and the top Schottky contact can be observed, resulting in a pinch off point, depicted as point A in Fig. 1(a). The charge coupling effect by the trench MOS structure can effectively reduce the electric field underneath the Schottky contact and minimize the reverse leakage current due to the energy barrier lowering effect. However, the reduced electric field at the Schottky interface is accompanied with a local electric field crowding at the

TABLE I
Key Device Parameters for C-TMBS and SR-TMBS Diodes

Parameters	C-TMBS	SR-TMBS
Width of trench (W_t)	4.0 μm	4.0 μm
Width of Mesa (W_m)	2.0 μm	2.0 μm
Thickness of epilayer (T_{epi})	9.0 μm	9.0 μm
Substrate doping (N_{sub})	5×10^{18} cm^{-3}	5×10^{18} cm^{-3}
Etch depth of trench (T_d)	2.0 μm	2.0 μm
Thickness of Oxide (T_{ox})	0.2 μm	0.2 μm
Thickness of Substrate (T_s)	2.0 μm	2.0 μm

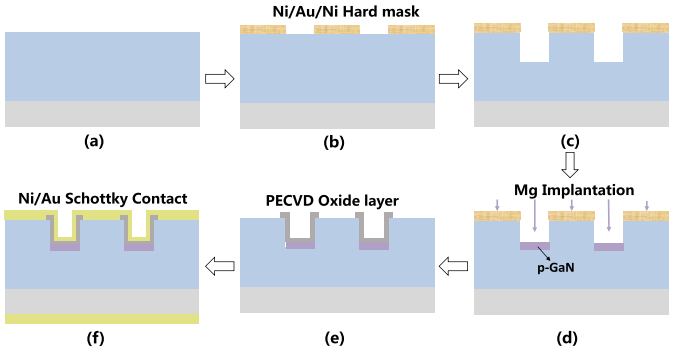

Fig. 2. Fabrication process of the GaN-based vertical TMBS diodes with p-GaN SRs. (a) MOCVD epitaxial layer. (b) Form Hard mask. (c) Trench etching. (d) Form p-GaN SRs. (e) Oxide deposition and patterning. (f) Metal evaporation.

mesa edges, which may result in a premature breakdown of the C-TMBS diodes. With p-GaN SRs, an additional coupling effect by the embedded p-n junction is involved and thus the pinch-off point is shifted downward from the original point A to point B in the SR-TMBS diodes in Fig. 1(b), leading to an enhanced 2-D depletion into the drift region. Detailed parameters of the devices are listed in Table I.

To demonstrate the fabrication feasibility of the proposed SR-TMBS structure, an assumed schematic process flow is presented in Fig. 2. To start with, a 9-μm-thick n^--GaN drift layer is epitaxially grown on freestanding n^+-GaN substrates. A Ni/Au/Ni hard mask is then selectively deposited to define the etching and implanting region. The trench structure is obtained by dry etching, followed by a self-aligned Mg implantation to form the p-type SRs at the bottom of the trench. After removal of the metal mask, a SiO_2 layer is deposited and openings are created on top of the mesa by dry etching. A Ni/Au metal stack is deposited to form the Schottky contact. Finally, the bottom Ohmic contact can be formed by e-beam deposition of Ti/Al stack. Similar structures have been demonstrated in [31]–[34], confirming the viability of the proposed fabrication process.

The doping, thickness, and width of the p-GaN SRs were varied to explore the optimal design parameters. Advanced Physical Models of Semiconductor Devices (APSYS) software [35] was used for numerical investigations. The key physical models used in the simulation include continuity and Poisson's equations, carrier generation–recombination model, intraband tunneling model, and drift-diffusion model. The breakdown process was determined by the impact ionization model, in which the impact ionization coefficients for GaN

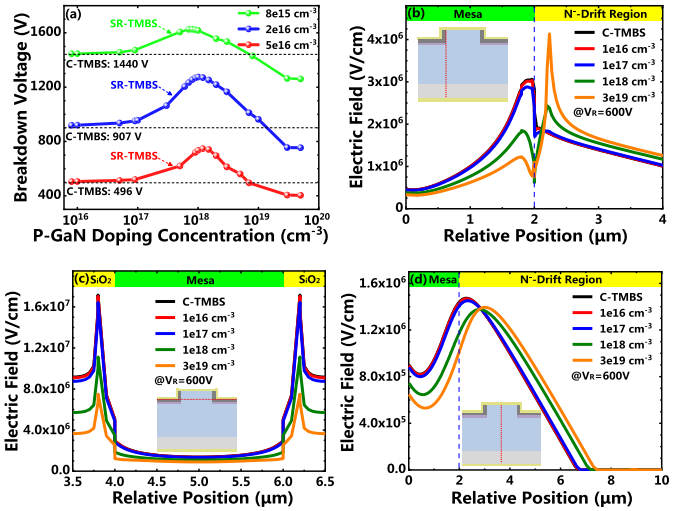

Fig. 3. (a) BV as a function of the p-GaN doping concentration for SR-TMBS diodes at an n-GaN drift doping concentration of 8e15, 2e16, and 5e16 cm^{-3}, respectively. (b) Electric field profiles along the oxide sidewall for the SR-TMBS diodes with different p-GaN doping concentrations at a reverse bias of 600 V (n^--GaN drift doping concentration: 2e16 cm^{-3}). (c) Lateral electric field profiles at the metal/oxide interface for the SR-TMBS diodes with different p-GaN doping concentrations (n-GaN drift doping concentration: 2e16 cm^{-3}). (d) Electric field profiles along the mesa midline for the SR-TMBS diodes with different p-GaN doping concentrations at a reverse bias of 600 V (n^--GaN drift doping concentration: 2e16 cm^{-3}).

were calculated by the following Chynoweth's equations (1) and (2) [29], [36]:

$$\alpha_n = 2.9 \times 10^8 \text{ cm}^{-1} \times e^{\left(\frac{-3.4\times10^7 \text{ V/cm}}{E}\right)} \quad (1)$$

$$\alpha_p = 1.34 \times 10^8 \text{ cm}^{-1} \times e^{\left(\frac{-2.03\times10^7 \text{ V/cm}}{E}\right)} \quad (2)$$

where E is defined as the magnitude of the electric field in the drift region of the devices at the reverse bias condition.

III. Result and Discussions

A. Impact of the p-GaN Doping Concentration on the Electrical Properties for GaN-Based SR-TMBS Diodes

Fig. 3(a) shows the influence of the p-GaN doping concentration on the breakdown characteristics of the SR-TMBS diodes with different background doping levels in the drift region. The BV was extracted when the reverse leakage current density reached 0.01 A/cm^2. The BV of the SR-TMBS diodes is reversely proportional to the background concentration in the drift region, mainly due to the reduced depletion width in the drift region at the reverse bias condition. The doping concentration of the p-GaN SRs has a significant impact on the breakdown characteristics of the SR-TMBS diodes. Note that the doping concentration refers to the concentration of the Mg dopant. The BV of the SR-TMBS diodes first increases and then decreases with increased doping concentration of the p-GaN SRs. A peak BV of 1281 V was recorded at a p-GaN doping concentration of 1×10^{18} cm^{-3} for the SR-TMBS diodes with a drift doping concentration of 2×10^{16} cm^{-3}. Further increase of the p-doping concentration to above 1×10^{19} cm^{-3} results in a BV even lower than that of the C-TMBS diodes. In addition, the optimal p-doping concentration that leads to the highest BV is positively correlated with the background doping level in the drift region. More specifically, the peak value of the BV is obtained at a p-doping concentration of 8×10^{17} cm^{-3}, 1×10^{18} cm^{-3}, and 1.2×10^{18} cm^{-3}, with a drift doping concentration of 8×10^{15} cm^{-3}, 2×10^{16} cm^{-3}, and 5×10^{16} cm^{-3}, respectively.

The BV is mainly determined by the electric field profiles and the depletion region width at reverse bias condition. Fig. 3(b) plots the vertical electric field profiles along the oxide/GaN interface, as shown by the dashed line in the inset. While the traditional C-TMBS diodes featured a single electric field peak adjacent to the mesa edges, two electric field peaks can be observed for the SR-TMBS diodes, which corresponds to the electric field crowding at the corner of the trench and the edge of the embedded p-GaN SRs, respectively. With a low doping concentration of 1×10^{16} cm^{-3} in the p-GaN SRs, only a negligible proportion of the electric field was coupled from the corner of the trench to the edge of the p-GaN SRs. As a result, the premature breakdown still takes place at the mesa edges and the BV remains nearly the same as the C-TMBS diodes. By increasing the p-type doping concentration to 1×10^{18} cm^{-3}, an uniformly distributed 2-D electric field profile can be observed, resulting in a peak BV of 1281 V in the SR-TMBS diodes. However, when we further increase the p-doping concentration to 3×10^{19} cm^{-3} in the embedded SRs, the electric field at the SR edge exceeds the critical field of GaN material and results in the breakdown of the device, which explains the even lower BV than that of the C-TMBS diodes. The lateral electric field profiles in Fig. 3(c) also indicate that as the concentration of p-GaN increases, the electric field at the metal/oxide interface in the vicinity of the trench corner decreases accordingly, which agrees with the increased electric field peak at the trench corner with increased p-GaN doping level in Fig. 3(b). Note that the peak value of the electric field at the metal/oxide interface in Fig. 3(c) is ten times the value at the oxide/GaN interface in Fig. 3(b), indicating that the electric field peaks at the oxide/GaN interface is inducted from the metal/oxide interface. Fig. 3(d) illustrates the electric field profiles along the midline of the mesa for the C-TMBS diodes and the SR-TMBS diodes with different p-GaN doping concentration. As the doping concentration of p-GaN increases, the peak position of the electric field profile moves from the Schottky interface into the bulk n^--GaN drift region and the surface electric field underneath the Schottky contact decreases, leading to a reduced reverse leakage current density of the SR-TMBS diodes. In addition, thanks to the charge coupling effect, an increased depletion width is observed with a larger p-doping concentration, which can also contribute to an improved breakdown capability.

B. Impact of p-GaN Thickness on the Electrical Properties for GaN-Based SR-TMBS Diodes

As has been discussed earlier, the doping concentration of the p-GaN SRs affects the BV of the SR-TMBS diodes via the electric field distribution. The basic principle toward

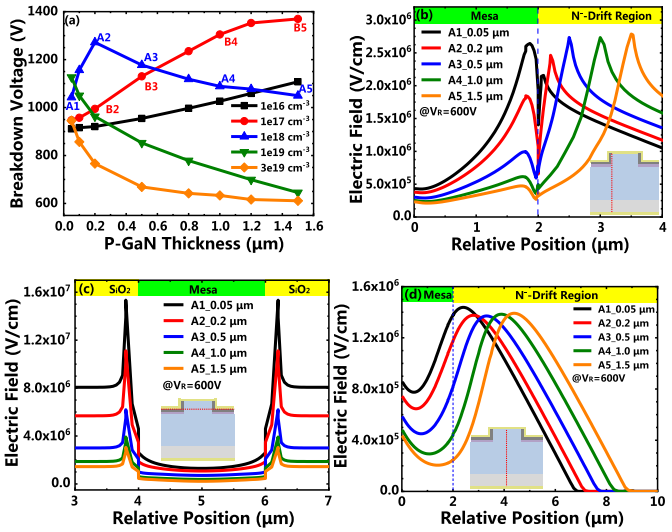

Fig. 4. (a) BV as a function of the p-GaN thickness and doping concentration in the SR-TMBS diodes. (b) Electric field profiles along the oxide sidewall for the SR-TMBS diodes with different p-GaN thicknesses at a reverse bias of 600 V. (c) Electric field profiles at the metal/oxide interface for the SR-TMBS diodes with different p-GaN thicknesses at a reverse bias of 600 V. (d) Electric field profiles along the mesa midline for the SR-TMBS diodes with different p-GaN thicknesses at a reverse bias of 600 V. The doping concentration of the n^--GaN drift layer is 2e16 cm^{-3}.

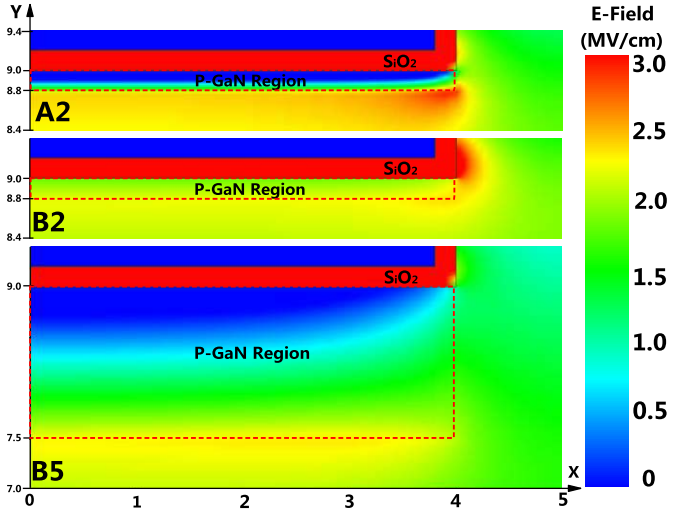

Fig. 5. 2-D electric field distribution of devices A2, B2, and B5 in the vicinity of the p-GaN SRs at a reverse bias of 900 V.

an improved BV is to achieve a uniform distribution of the electric field at reverse bias. In addition to the doping concentration, the thickness of the p-GaN SRs also plays a crucial role in the electric field distribution. The relationship between the thickness of the p-GaN SRs and the BV of the SR-TMBS diodes is shown in Fig. 4(a). Subject to different p-GaN doping concentration, the impact of the p-GaN thickness on the BV varies. At a p-GaN doping level exceeding 1×10^{19} cm^{-3}, the BV of the device decreases monotonously with the thickness. When the p-GaN doping concentration is set to 1×10^{18} cm^{-3}, the BV first increases to a peak value (1281 V for device A2) at a thickness of 200 nm and then decreases with increased p-GaN thickness. As the p-doping concentration reduces to 1×10^{17} cm^{-3}, the BV increased monotonously with the p-GaN thickness and the highest BV of ~1400 V was obtained for device B5 at a p-GaN thickness of 1.5 μm. Further decrease in the p-doping concentration to 1×10^{16} cm^{-3} leads to an overall reduction in the BV, which has been discussed in Fig. 3. Now that both the doping concentration and the thickness of the p-GaN SRs poses a significant impact on the BV, a simultaneous optimization of the two adjunct parameters is highly desired to achieve the optimal device performance.

To explore the mechanism behind these phenomena, we extracted the electric field profiles from the SR-TMBS diodes along selected cutlines at a reverse bias of 600 V. Fig. 4(b) plots the vertical electric field profiles along the oxide/GaN interface for the SR-TMBS diodes with a p-doping concentration of 1×10^{18} cm^{-3} in the embedded SRs. With increased p-GaN thickness, the electric field is gradually redistributed from the trench corners to the edge of the p-GaN SR structure. Most uniform distributions can be achieved with a p-GaN thickness of 200 nm (device A2). Smaller or larger p-GaN thickness will result in a premature breakdown either at the trench corners or the p-GaN SR edges due to electric field crowding. The redistribution of the electric field with different p-GaN thickness can also be confirmed from Fig. 4(c), in which a substantial decrease in the peak electric field at the metal/oxide interface close to the trench corner can be observed with increased p-GaN thickness. The thickness of the embedded p-GaN SRs is also closely related to the electric field value at the surface and the depletion depth, as is shown in Fig. 4(d). An increased p-GaN thickness can result in a reduced electric field at the Schottky surface and an increased depletion width, which can be correlated with an alleviated reverse leakage current of the SR-TMBS diodes.

For the purpose of demonstrating the redistribution process of the electric field with embedded p-GaN SRs, we compare the 2-D electric field of the SR-TMBS diodes with different p-GaN doping concentration and thickness in Fig. 5. Devices A2 and B2 are designed with the same p-GaN thickness but different doping concentrations (1×10^{18} cm^{-3} and 1×10^{17} cm^{-3}, respectively). It can be seen that the electric field peak is successfully transferred from the trench corners (device B2) to the edges of the p-GaN SRs (device A2), which agrees well with the 1-D electric field distribution in Fig. 4(b) and (c). Devices B2 and B5 consist of the same p-GaN doping concentration but different thicknesses (200 nm and 1.5 μm, respectively). With a larger p-GaN thickness in device B5, the electric field crowding at the trench corners (device B2) can be effectively alleviated. In the meantime, a uniformly distributed electric field can be recorded across the embedded thick p-GaN SRs. As a result, the commonly observed electric field crowding at the SRs is also negligible for device B5, which leads to an enhanced BV, compared to device A2. From the discussion above, we can draw the conclusion that both the p-GaN concentration and the thickness can influence the electric field distribution at reverse bias.

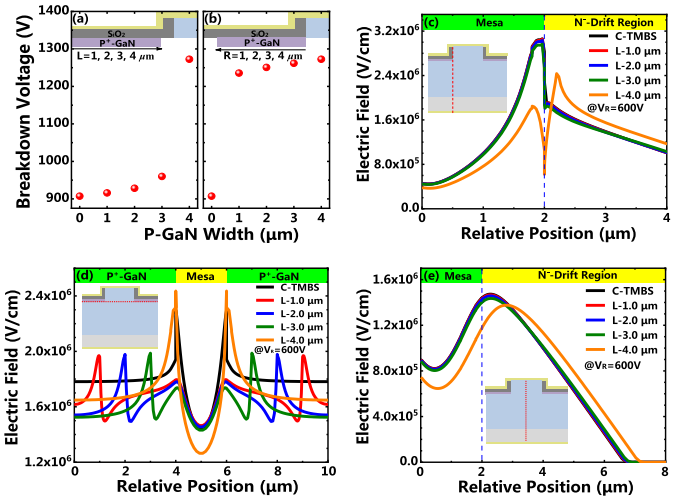

Fig. 6. (a) and (b) BV as a function of the width of p-GaN SRs in the SR-TMBS diodes. (c) Electric field profiles along the oxide sidewall for the SR-TMBS diodes with different p-GaN widths at a reverse bias of 600 V. (d) Electric field profiles at the bottom of the p-GaN SRs for the SR-TMBS diodes with different p-GaN widths at a reverse bias of 600 V. (e) Electric field profiles along the mesa midline for the SR-TMBS diodes with different p-GaN widths at a reverse bias of 600 V. The doping concentration of the n^--GaN drift layer is 2e16 cm^{-3}.

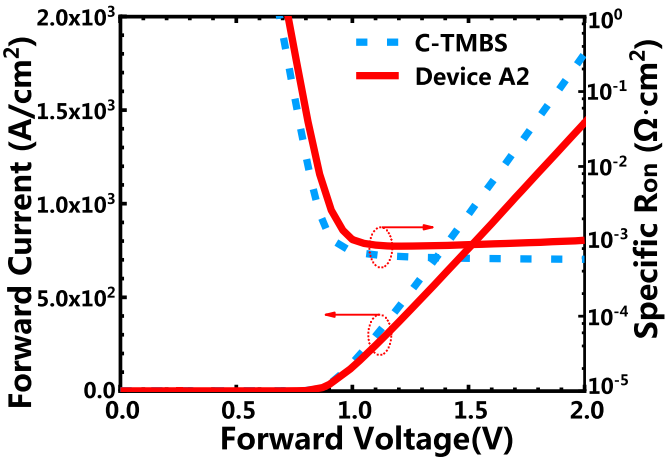

Fig. 7. Forward current density and specific ON-resistance as a function of forward voltage for the C-TMBS diodes and optimized SR-TMBS diodes (device A2).

C. Impact of p-GaN Width on the Electrical Properties for GaN-Based SR-TMBS Diodes

After addressing the impact of the p-GaN concentration and thickness on the breakdown performance of the SR-TMBS diodes, we then look into how the p-GaN width affects the electric field distribution and the BV of the SR-TMBS diodes. As is shown in Fig. 6(a) and (b), two groups of SR-TMBS structures are designed to elucidate the relationship between the width of p-GaN SRs and the charge coupling effect. In more detail, group A consists of p-GaN SRs that extends from the edge of the device to the corner of the trench, while group B features p-GaN SRs that fills the region from the trench corner to the edge of the devices. The lateral width of the embedded p-GaN SRs for groups A and B is 1, 2, 3, and 4 μm, respectively. Fig. 6(a) and (b) illustrates the influence of the p-GaN width on the BV in groups A and B, respectively. With increased p-GaN width toward the trench corners in group A, the BV improves moderately from 907 V for the C-TMBS diodes to 960 V for the SR-TMBS diodes with a 3-μm-wide SR, until an abrupt increase to 1272 V occurred in the SR-TMBS diodes with a lateral SR width of 4 μm (the same width as the trench). In terms of group B in Fig. 6(b), only a marginal improvement in the BV can be observed with increased SR width, from which a conclusion can be drawn that the p-GaN SRs adjacent to the mesa edges plays a more pivotal role than that close to the edge of the device.

To further investigate the influence of the p-GaN width and location on the breakdown characteristics of the SR-TMBS diodes, we plotted the electric field profiles from the devices in group A. Fig. 6(c) presents the electric field distribution along the oxide/GaN sidewall for the SR-TMBS diodes with different p-GaN width. The SR-TMBS diodes with a p-GaN width from 1 to 3 μm featured almost the same electric field profiles as that of the C-TMBS diodes, which explains the negligible breakdown improvement with 1 μm to 3 μm p-GaN SRs in Fig. 6(a). On the other hand, an obvious redistribution of the electric field toward a uniform profile can be observed for the SR-TMBS diodes with a 4 μm p-GaN SR, leading to a dramatic enhancement in the BV. Fig. 6(d) shows the lateral electric field profiles extracted from the p-GaN/n^--GaN interface of the SR-TMBS diodes with different p-GaN widths. The peak position of the electric field profiles locates at the edges of the embedded SRs and shifts to the corner of the trench with increased p-GaN width. The highest electric field can be observed for SR-TMBS diodes with a p-GaN width of 4 μm, indicating an effective redistribution of the electric field from the trench corner to the p-GaN edges. Afterward, the vertical electric field profiles along the mesa midline for the SR-TMBS diodes with different p-GaN widths are represented in Fig. 6(e). The surface electric field under the Schottky contact can be reduced and the depletion width is also increased, which is related to the enhanced charge coupling effect with wider p-GaN SRs toward the trench corner.

D. on-Resistance and Baliga's Figure of Merit (FOM) for GaN-Based SR-TMBS Diodes

Based on the optimization above, we achieved an optimal SR-TMBS diode (device A2) with a BV of 1281 V, which features a 41% enhancement in the BV, when compared to the C-TMBS diodes (907 V). Despite a larger BV obtained for device B5, it is challenging to fabricate the SR-TMBS diodes with a 1.5-μm-thick p-GaN SR by ion implantation. The key design parameters for device A2 include a p-GaN thickness of 200 nm, a p-GaN width of 4 μm, a p-doping concentration of 1×10^{18} cm^{-3}, and a background doping level of 2×10^{16} cm^{-3}, which are experimentally achievable and feasible. The forward I–V characteristics and specific ON-resistance for device A2 and the C-TMBS diodes are shown in Fig. 7. A turn-on voltage of ~0.7 V is obtained for both devices, indicating similar Schottky barrier height for the C-TMBS and SR-TMBS diodes. The forward current was normalized

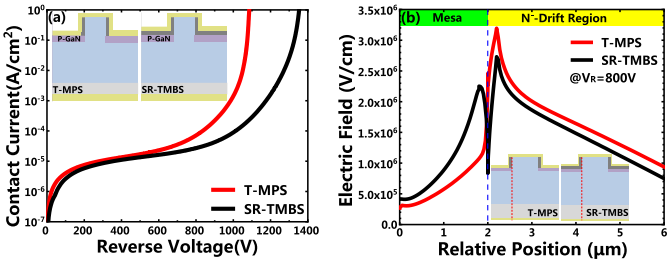

Fig. 8. (a) Reverse characteristics and device structure diagrams of the SR-TMBS diodes and the T-MPS diodes. (b) Electric field profiles along the oxide sidewall for the SR-TMBS diodes and the T-MPS diodes at a reverse bias of 800 V.

by the effective area of each device. The forward current path of the SR-TMBS diodes is narrower than the C-TMBS diodes due to embedded p-n junction. Therefore, the specific ON-resistance of device A2 (0.78 mΩ·cm^2) is slightly larger than that of the C-TMBS diodes (0.58 mΩ·cm^2). In order to discuss the application potential of the SR-TMBS diodes in power systems, we compare Baliga's figure of merit (FOM) of the C-TMBS diodes and SR-TMBS diodes. Thanks to the largely improved BV, the FOM of the SR-TMBS diodes is calculated to be 2.1 GW/cm^2, which is 50% higher than C-TMBS diodes (1.4 GW/cm^2). The FOM of the SR-TMBS diodes can be further improved by optimizing the design of the channel region [32]–[34], which can compensate the increased ON-resistance due to the embedded p-GaN SRs without degrading the breakdown performance.

E. Further Structural Optimization of the SR-TMBS Diodes Toward Avalanche Capability

While the proposed SR-TMBS diodes feature a dramatic enhancement in Baliga's FOM, one pivotal challenge remains to be tackled. With the oxide layer sandwiched between the embedded p-GaN and the anode metal, the holes cannot be effectively removed during the avalanche process, which deprives the devices of the avalanche capability to withstand the transient overcurrent under the circumstances of current overshoot or oscillation [37], [38]. By removing the oxide spacer layer and forming an Ohmic contact with the p-GaN SRs, the minority carrier injection can be made possible, and the avalanche capability can be achieved in the vertical GaN power devices, allowing for the superior device reliability [39]–[42].

To investigate the influence of the oxide spacer layer on the device performance, we established trench merged p-i-n Schottky (T-MPS) diode structures and compared their reverse characteristics with the SR-TMBS diodes (device A2). The schematic structures and reverse I–V curves can be found in Fig. 8(a). For a fair comparison, the key parameters for the two structures are kept identical, except that the oxide spacers are removed for the T-MPS diodes. At a reverse leakage current density of 0.01 A/cm^2, a minor degradation in the BV can be observed from 1281 V in the SR-TMBS diodes to 1050 V in the T-MPS diodes.

For the purpose of clarifying the mechanism behind the inferior breakdown characteristics in the T-MPS diodes, we plotted the electric field profiles along the vertical sidewall of the mesa, as shown by the dashed lines in the inset of Fig. 8(b). Under a reverse bias of 800 V, a single peak can be observed in the electric field profile of the T-MPS diodes, with the peak value exceeding the critical field of the GaN materials (~3 MV/cm), which results in a premature breakdown of the devices. On the other hand, the SR-TMBS diodes feature a more uniform double-peak electric field profile, thanks to the joint depletion effects from the oxide and p-GaN SRs. As a result, the T-MPS diodes feature a marginally lower BV than that of the SR-TMBS diodes. Therefore, the proposed SR-TMBS structure can be further optimized to achieve avalanche capability at a small price of a slightly lower BV, which can mark a major step forward for GaN vertical power Schottky diodes toward high-voltage, high-power, and high-reliability power system applications.

IV. Conclusion

In summary, we report GaN trench MOS SBDs with embedded p-GaN SRs and implement systematic parametric analysis of the devices by numerical simulation. The incorporation of the p-GaN SRs can lead to enhanced charge coupling effect and thus an uniformly redistributed electric field profile at revers bias. As a result, the BV of conventional TMBS can be enhanced by 41% to 1281 V, subject to an optimal set of parameters for the embedded p-GaN SRs. In the meantime, only a minor increase in the specific ON-resistance can be observed for the SR-TMBS diodes. The results are very promising for the future adoption of GaN vertical Schottky didoes toward an all-GaN power electronic systems for high-speed, high-voltage, and high-power applications.

Acknowledgment

The authors would like to thank H. Wang, J. Yin, and X. Liu for their valuable discussion and technical support.

References

[1] J. Ma and E. Matioli, "High performance tri-gate GaN power MOSHEMTs on silicon substrate," *IEEE Electron Device Lett.*, vol. 38, no. 3, pp. 367–370, Mar. 2017, doi: 10.1109/LED.2017.2661755.

[2] W. Zhang, J. Zhang, M. Xiao, L. Zhang, and Y. Hao, "$Al_{0.3}Ga_{0.7}N$/GaN (10 nm)/$Al_{0.1}Ga_{0.9}N$ HEMTs with low leakage current and high three-terminal breakdown voltage," *IEEE Electron Device Lett.*, vol. 39, no. 9, pp. 1370–1372, Sep. 2018, doi: 10.1109/LED.2018.2859438.

[3] H. Jiang, Q. Lyu, R. Zhu, P. Xiang, K. Cheng, and K. M. Lau, "1300 V normally-OFF p-GaN gate HEMTs on Si with high ON-state drain current," *IEEE Trans. Electron Devices*, vol. 68, no. 2, pp. 653–657, Feb. 2021, doi: 10.1109/TED.2020.3043213.

[4] M. Xiao *et al.*, "3.3 kV multi-channel AlGaN/GaN Schottky barrier diodes with P-GaN termination," *IEEE Electron Device Lett.*, vol. 41, no. 8, pp. 1177–1180, Aug. 2020, doi: 10.1109/LED.2020.3005934.

[5] J.-G. Kim, C. Cho, E. Kim, J. S. Hwang, K.-H. Park, and J.-H. Lee, "High breakdown voltage and low-current dispersion in AlGaN/GaN HEMTs with high-quality AlN buffer layer," *IEEE Trans. Electron Devices*, vol. 68, no. 4, pp. 1513–1517, Apr. 2021, doi: 10.1109/TED.2021.3057000.

[6] J. P. Kozak, R. Zhang, Q. Song, J. Liu, W. Saito, and Y. Zhang, "True breakdown voltage and overvoltage margin of GaN power HEMTs in hard switching," *IEEE Electron Device Lett.*, vol. 42, no. 4, pp. 505–508, Apr. 2021, doi: 10.1109/LED.2021.3063360.

[7] M. Xiao, Y. Ma, K. Liu, K. Cheng, and Y. Zhang, "10 kV, 39 mΩ ·cm^2 multi-channel AlGaN/GaN Schottky barrier diodes," *IEEE Electron Device Lett.*, vol. 42, no. 6, pp. 808–811, Jun. 2021, doi: 10.1109/LED.2021.3076802.

[8] J. Ma, G. Kampitsis, P. Xiang, K. Cheng, and E. Matioli, "Multi-channel tri-gate GaN power Schottky diodes with low ON-resistance," *IEEE Electron Device Lett.*, vol. 40, no. 2, pp. 275–278, Feb. 2019, doi: 10.1109/LED.2018.2887199.

[9] B. Jogai, "Influence of surface states on the two-dimensional electron gas in AlGaN/GaN heterojunction field-effect transistors," *J. Appl. Phys.*, vol. 93, pp. 1631–1635, Feb. 2003, doi: 10.1063/1.1530729.

[10] Y. Zhang and T. Palacios, "(Ultra) wide-bandgap vertical power FinFETs," *IEEE Trans. Electron Devices*, vol. 67, no. 10, pp. 3960–3971, Oct. 2020, doi: 10.1109/TED.2020.3002880.

[11] Y. Zhang *et al.*, "GaN FinFETs and trigate devices for power and RF applications: Review and perspective," *Semicond. Sci. Technol.*, vol. 36, no. 5, May 2021, Art. no. 054001, doi: 10.1088/1361-6641/abde17.

[12] R. A. Khadar, C. Liu, R. Soleimanzadeh, and E. Matioli, "Fully vertical GaN-on-Si power MOSFETs," *IEEE Electron Device Lett.*, vol. 40, no. 3, pp. 443–446, Mar. 2019, doi: 10.1109/LED.2019.2894177.

[13] C. Liu, R. A. Khadar, and E. Matioli, "GaN-on-Si quasi-vertical power MOSFETs," *IEEE Electron Device Lett.*, vol. 39, no. 1, pp. 71–74, Jan. 2018, doi: 10.1109/LED.2017.2779445.

[14] C. Liu, R. A. Khadar, and E. Matioli, "Vertical GaN-on-Si MOSFETs with monolithically integrated freewheeling Schottky barrier diodes," *IEEE Electron Device Lett.*, vol. 39, no. 7, pp. 1034–1037, Jul. 2018, doi: 10.1109/LED.2018.2841959.

[15] Y. Zhang *et al.*, "Large-area 1.2-kV GaN vertical power FinFETs with a record switching figure of merit," *IEEE Electron Device Lett.*, vol. 40, no. 1, pp. 75–78, Jan. 2019. doi: 10.1109/LED.2018.2880306.

[16] X. Guo *et al.*, "High-voltage and high-I_{ON}/I_{OFF} quasi-vertical GaN-on-Si Schottky barrier diode with argon-implanted termination," *IEEE Electron Device Lett.*, vol. 42, no. 4, pp. 473–476, Apr. 2021, doi: 10.1109/LED.2021.3058380.

[17] Y. Li *et al.*, "Quasi-vertical GaN Schottky barrier diode on silicon substrate with 10^{10} high on/off current ratio and low specific on-resistance," *IEEE Electron Device Lett.*, vol. 41, no. 3, pp. 329–332, Mar. 2020, doi: 10.1109/LED.2020.2968392.

[18] S. Han, S. Yang, and K. Sheng, "High-voltage and high-I_{ON}/I_{OFF} vertical GaN-on-GaN Schottky barrier diode with nitridation-based termination," *IEEE Electron Device Lett.*, vol. 39, no. 4, pp. 572–575, Apr. 2018, doi: 10.1109/LED.2018.2808684.

[19] S. Han, S. Yang, and K. Sheng, "Fluorine-implanted termination for vertical GaN Schottky rectifier with high blocking voltage and low forward voltage drop," *IEEE Electron Device Lett.*, vol. 40, no. 7, pp. 1040–1043, Jul. 2019, doi: 10.1109/LED.2019.2915578.

[20] L. Nela, R. Van Erp, G. Kampitsis, H. K. Yildirim, J. Ma, and E. Matioli, "Ultra-compact, high-frequency power integrated circuits based on GaN-on-Si Schottky barrier diodes," *IEEE Trans. Power Electron.*, vol. 36, no. 2, pp. 1269–1273, Feb. 2021, doi: 10.1109/TPEL.2020.3008226.

[21] E. Bahat-Treidel *et al.*, "Fast-switching GaN-based lateral power Schottky barrier diodes with low onset voltage and strong reverse blocking," *IEEE Electron Device Lett.*, vol. 33, no. 3, pp. 357–359, Mar. 2012, doi: 10.1109/LED.2011.2179281.

[22] Z. Bian *et al.*, "Leakage mechanism of quasi-vertical GaN Schottky barrier diodes with ultra-low turn-on voltage," *Appl. Phys. Exp.*, vol. 12, no. 8, Aug. 2019, Art. no. 084004, doi: 10.7567/1882-0786/ab3297.

[23] Y. Zhang *et al.*, "Vertical GaN junction barrier Schottky rectifiers by selective ion implantation," *IEEE Electron Device Lett.*, vol. 38, no. 8, pp. 1097–1100, Aug. 2017, doi: 10.1109/LED.2017.2720689.

[24] W. Li *et al.*, "Design and realization of GaN trench junction-barrier-Schottky-diodes," *IEEE Trans. Electron Devices*, vol. 64, no. 4, pp. 1635–1641, Apr. 2017, doi: 10.1109/TED.2017.2662702.

[25] T. Hayashida, T. Nanjo, A. Furukawa, T. Watahiki, and M. Yamamuka, "Leakage current reduction of vertical GaN junction barrier Schottky diodes using dual-anode process," *Jpn. J. Appl. Phys.*, vol. 57, no. 4, Feb. 2018, Art. no. 040302, doi: 10.7567/JJAP.57.040302.

[26] B. J. Baliga, *Advanced Power Rectifier Concepts*. New York, NY, USA: Springer, 2009, doi: 10.1007/978-0-387-75589-2.

[27] K. Hasegawa, G. Nishio, K. Yasunishi, N. Tanaka, N. Murakami, and T. Oka, "Vertical GaN trench MOS barrier Schottky rectifier maintaining low leakage current at 200 °C with blocking voltage of 750 V," *Appl. Phys. Exp.*, vol. 10, no. 12, Dec. 2017, Art. no. 121002, doi: 10.7567/APEX.10.121002.

[28] K. Sasaki *et al.*, "First demonstration of Ga_2O_3 trench MOS-type Schottky barrier diodes," *IEEE Electron Device Lett.*, vol. 38, no. 6, pp. 783–785, Jun. 2017, doi: 10.1109/LED.2017.2696986.

[29] X. Jia *et al.*, "Design strategies for mesa-type GaN-based Schottky barrier diodes for obtaining high breakdown voltage and low leakage current," *IEEE Trans. Electron Devices*, vol. 67, no. 5, pp. 1931–1938, May 2020, doi: 10.1109/TED.2020.2978007.

[30] Y. Zhang *et al.*, "Trench formation and corner rounding in vertical GaN power devices," *Appl. Phys. Lett.*, vol. 110, no. 19, May 2017, Art. no. 193506, doi: 10.1063/1.4983558.

[31] Y. Zhang *et al.*, "Novel GaN trench MIS barrier Schottky rectifiers with implanted field rings," in *IEDM Tech. Dig.*, Dec. 2016, pp. 10.2.1–10.2.4, doi: 10.1109/IEDM.2016.7838386.

[32] K. Tian *et al.*, "An improved 4H-SiC trench-gate MOSFET with low ON-resistance and switching loss," *IEEE Trans. Electron Devices*, vol. 66, no. 5, pp. 2307–2313, May 2019, doi: 10.1109/TED.2019.2905636.

[33] Y. Wang, W.-J. Wang, C.-H. Yu, Y.-F. Huang, Y.-L. Sun, and J.-X. Tang, "An optimized 4H-SiC trench MOS barrier Schottky (TMBS) rectifier," *IEEE J. Electron Devices Soc.*, vol. 6, pp. 1154–1158, Sep. 2018, doi: 10.1109/JEDS.2018.2871066.

[34] F. Cao, M.-T. Bao, X. Wu, W.-J. Wang, C.-H. Yu, and Y. Wang, "An improved 4H-SiC trench MOS barrier Schottky diode with lower on-resistance," *IEEE Access*, vol. 7, pp. 95710–95715, Jul. 2019, doi: 10.1109/ACCESS.2019.2927231.

[35] Crosslight Software Inc. *APSYS 2018 and APSYS Technical Manuals*. Accessed: Sep. 6, 2021. [Online]. Available: https://www.crosslight.com

[36] V. K. Sundaramoorthy and I. Nistor, "Study of edge termination structures for high power GaN Schottky diodes," *Phys. Status Solidi C*, vol. 8, nos. 7–8, pp. 2270–2272, May 2011, doi: 10.1002/pssc.201001032.

[37] L. Knoll *et al.*, "Robust 3.3 kV silicon carbide MOSFETs with surge and short circuit capability," in *Proc. 29th Int. Symp. Power Semiconductor Devices IC's (ISPSD)*, May 2017, pp. 243–246, doi: 10.23919/ISPSD.2017.7988905.

[38] L. Liu *et al.*, "Investigation of avalanche capability of 1200 V 4H-SiC MPS diodes and JBS diodes," in *Proc. 32nd Int. Symp. Power Semiconductor Devices ICs (ISPSD)*, Sep. 2020, pp. 210–213, doi: 10.1109/ISPSD46842.2020.9170067.

[39] K. Nomoto *et al.*, "1.7-kV and 0.55-m$\Omega \cdot cm^2$ GaN p-n diodes on bulk GaN substrates with avalanche capability," *IEEE Electron Device Lett.*, vol. 37, no. 2, pp. 161–164, Feb. 2016, doi: 10.1109/LED.2015.2506638.

[40] J. Liu *et al.*, "Trap-mediated avalanche in large-area 1.2 kV vertical GaN p-n diodes," *IEEE Electron Device Lett.*, vol. 41, no. 9, pp. 1328–1331, Sep. 2020, doi: 10.1109/LED.2020.3010784.

[41] J. Liu *et al.*, "Surge current and avalanche ruggedness of 1.2-kV vertical GaN p-n diodes," *IEEE Trans. Power Electron.*, vol. 36, no. 10, pp. 10959–10964, Oct. 2021, doi: 10.1109/TPEL.2021.3067019.

[42] J. Liu *et al.*, "1.2-kV vertical GaN fin-JFETs: High-temperature characteristics and avalanche capability," *IEEE Trans. Electron Devices*, vol. 68, no. 4, pp. 2025–2032, Apr. 2021, doi: 10.1109/TED.2021.3059192.